A 3D model of three phase shunt reactors by using a finite element technique with coupling to global quantities

Hung Bui Duc[1], Tu Pham Minh[1], Bao Doan Thanh[2], Duc-Quang Nguyen[3], Vuong Dang Quoc[1]
[1]Department of Electrical Engineering, Hanoi University of Science and Technology, Hanoi, Viet Nam
[2]Faculty of Engineering and Technology, Quy Nhon University, Binh Dinh, Viet Nam
[3]Faculty of Electrical Engineering, Electric Power University, Hanoi, Viet Nam

Article Info

Article history:

Received Feb 5, 2023
Revised Apr 12, 2023
Accepted Apr 17, 2023

Keywords:

Air core reactor
Copper loss
Finite element method
Iron loss
Shunt reactor

ABSTRACT

The finite element technique is used widely for researchers and manufacturers to design and simulate electrical systems in general and electrical machines such as shunt reactors (SRs) and transformers in particular. Many papers have recently applied several methods to analyze magnetic fields, copper losses and joule power losses in the shunt reactors (SRs). In this research, the finite element technique with coupling to global quantities is proposed to investigate the voltage and current distributions in the windings, and compute the distribution of magnetic field in the air gap and along the air core of the SR, as well as copper and core losses. The developed method is directly applied to the practical SR of 91 MVAr and a rated voltage of 500 kV. The finite element method (FEM)-simulated results are validated with experimental results to ensure accuracy and reliability. This facilitate designing the reactor.

Corresponding Author:

Hung Bui Duc
Department of Electrical, Hanoi University of Science and Technology
No. 1 Dai Co Viet Street, Hai Ba Trung District, Hanoi, Viet Nam
Email: hung.buiduc@hust.edu.vn

1. INTRODUCTION

Nowadays, the shunt reactor (SR) is widely applied to stabilize the electrical systems due to parasitic capacitance appearing in the transmission line. It is also applied to bound the short-circuit current and overvoltage in the electrical system. In addition, it can be also used to imbibe not only the reactive power created by a conductive capacitance in power transmission lines, but also adjust the reactive power in the electrical system. Recently, several studies have presented the many different method to investigate and analyse electromagnetic parameters of the SR [1]-[10]. In reference [1], the finite element method (FEM) was presented to investigate the flux fringing distribution around the air gap of the magnetic circuit of the SR. In reference [2], the theory of Maxwell stress tensor was proposed to evaluate the electromagnetic force on the core blocks causing the vibration and noise during the working of SRs. In reference [3], the paper investigated the influence of distance air-gaps on the iron-core of SRs by using the analytical method. In this work, the winding inductance was also computed to define the relationship of the distance between the air gaps. In references [4], [5], a mathematical model was studied to consider the nonlinear dynamic case. In references [6], [7], the relation between the SR and power system in various transient situations was investigated. In reference [8], the effects of core block numbers on the inductance was studied via the analytical technique. In reference [9], a FEM was presented to compute the magnetic flux density distribution and losses in the magnetic circuit of the SR. In reference [10], [11], the papers provided a useful tool for the design and optimization of ferromagnetic-core inductors, which are commonly used in a variety of electronic devices. The analytical model presented can help engineers to reduce the time and cost involved in designing these devices while ensuring that the design meets the required specifications. In reference [12], this paper provides valuable insights into the use of air gaps in power inductor design. By understanding the influence of air-gap arrangements on inductor performance, designers can create more efficient and reliable inductors for a variety of applications.

It can be seen that the above studies have not investigated the voltage and current distributions on the windings, magnetic flux density on core blocks and in air gap between core blocks. In addition, the inductances of each winding phase has been not also considered in the previous studies. In this research, a FEM is developed to compute and design an oil-immersed SR of 91 MVAr, 50 Hz, 500 kV. The scenario of this paper is divided into two senarios. In the first approach, an analytic model is developed to define the desired output parameters of the proposed SR. In the second approach, a FEM is developed with the obtained parameters in the first step to compute and analyse the voltage and current distribution, magnetic flux density distribution, Joule power loss density and winding inductances. The simulated results of the FEM are verified with the experimental results to validate on the proposed method.

2. ANALYTICAL APPROACH OF THE SR

One of the most important things in designing the SR is the factor of the air gap volume. This factor depends on parameters of the SR, i.e. reactive power, magnetic flux distribution in the magnetic circuit, winding inductances, power frequency, and energy stored in the air gaps and the windings. For the SR, the reactive power (Q) is determined as (1) [1], [10], [13].

$$Q = U_{ef} I_{ef} \tag{1}$$

Where U_{ef} and I_{ef} are respectively the effecitive voltage and current. It should be noted that the resistance of windings is small in comparison with inductances, therefore this value can be ignored. For that, the electromagnetic force (EMF) and effective current are determined as (2) and (3) [13].

$$E_{ef} \approx U_{ef} = \left(\frac{2\pi}{\sqrt{2}}\right).f.N.B_m.A_{gap} \tag{2}$$

$$I = \frac{R_{gap}}{N} = \left(\frac{1}{\sqrt{2}}\right).\frac{B_m.l_{gap}}{\mu_0.N} \tag{3}$$

Where f is the frequency, N is the turn number, B_m is the maximum flux density, A_{gap} is the area of the air gap, l_{gap} is the length of the air gap, μ_0 is the air permeability and R_{gap} is the air gap reluctance. Based on (2) and (3), the air gap volume V_{gap} can be presented via the air gap length l_{gap}:

$$V_{gap} = A_{gap}.l_{gap} = \frac{Q}{\frac{\pi}{\mu_0}.f.B_m^2} \tag{4}$$

the air gap volume is considered as a constant if the quantity Q, magnetic flux and frequence are the constant. Therefore, the dimension of core (D_c) is determined as (5) [14], [15].

$$D_c = \sqrt{\frac{4.A_g}{\pi}} \tag{5}$$

The inductance of winding is calculated via the reactive power and voltage as (6).

$$L = \frac{U_{ef}^2}{\omega Q} \tag{6}$$

The size of the SR is influenced by the air gap length and area. Thus, the iron losses, copper losses and other factors depend on the different ratio value of the area and air gap length. Because this factor will decide to the cost and losses of the SR. The air gap permeance can be defined as (7) [16].

$$P_{gap} = \left(\frac{A_{gap}}{l_{gap}}\right)\mu_0 = P_g \tag{7}$$

The relation between the winding inductance and air gap permeance is:

$$L = N^2.P_g \quad (8)$$

the winding inductance can also be computed via the expression as (9) [10], [13].

$$L = \left(\frac{E_{eff}^2}{\mathrm{w.f}}\right) \quad (9)$$

From (8) and (9), one gets (10).

$$N = \sqrt{\frac{L}{\mu_0.(\frac{A_{gap}}{l_{gap}})}} = \frac{E_{eff}}{\sqrt{w.f.\mu_0.(\frac{A_{gap}}{l_{gap}})}} \quad (10)$$

3. FINITE ELEMENT APPROACH

3.1. Canonical magnetodynamic model

A model of a studied problem with a studied domain $\Omega = \Omega_c \cup \Omega_C^c$ (where domain Ω_c is the conducting region and and Ω_C^c is the non-conducting region) is presented in Figure 1. The boundary of Ω denotes $\partial\Omega = \Gamma = \Gamma_h \cup \Gamma_e$). The set of Maxwell's equations and behavior laws are written in the frequency domain as [10]:

$$rot\ H = J_s \quad (11)$$

$$rot\ E = -j\omega\ B \quad (12)$$

$$div\ B = 0 \quad (13)$$

$$B = \mu H \quad (14)$$

$$J = \sigma E \quad (15)$$

where H: the magnetic field (A/m), B: magnetic flux density, E: electric field (V/m), J_s: electric current density (A/m^2), J: eddy current density (A/m^2), μ: relative permeability, and σ: electric conductivity (S/m).

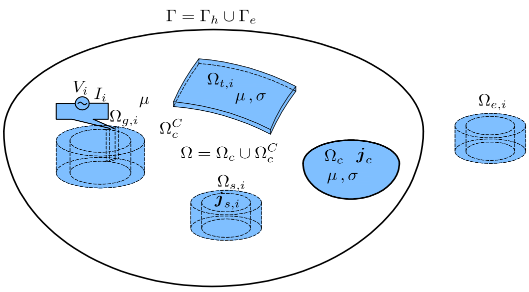

Figure 1. General magnetodynamic model [10]

These fields defined in function spaces (H_h $(rot;\Omega)$ and H_e $(rot;\Omega)$ must satisfy Tonti's diagram [10]. These function spaces contain the fields defined on Γ_h and Γ_e of the studied domain and BCs on Γ as (16) and (17) [10], [17]–[20].

$$n \times H|_{\Gamma_h} = 0 \quad (16)$$

$$n \cdot B|_{\Gamma_e} = 0 \quad (17)$$

Where n is the unit normal exterior to Ω. The set of (11), (12), and (13) is solved with the BCs in (14) and (15). In addition, global quantities with the current (I_i) and voltage (V_i) imposed the inductor are shown in Figure 2. The source of electromotive force (EMF) is defined through the surface $\Gamma_{g,i}$, i.e. (18) and (19) [8], [21].

$$\oint_{\Gamma_{g,i}^-}^{\Gamma_{g,i}^+} E \cdot dl = V_i \tag{18}$$

$$\oint_{\Gamma_{g,i}^-}^{\Gamma_{g,i}^+} n \cdot J \, ds = I_i \tag{19}$$

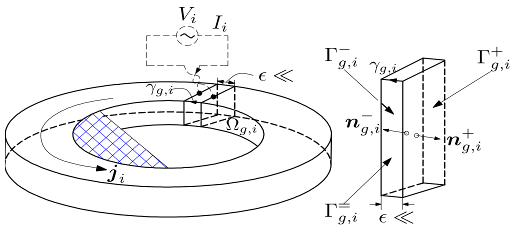

Figure 2. Magnetodynamic model with global quantities (current and voltage) [10]

3.2. Magnetic vector potential weak formulations

The magnetic vector potential weak formulation (A) ($B = \text{curl}\, A$ and $E = \sigma\partial_t A - \sigma \text{grad}\, \nu$) is defined via the Ampere's law (10 A) in Ω [10], [22]–[24].

$$\left(\frac{1}{\mu}\text{curl}\, A, \text{curl}\, w'\right)_\Omega + (\sigma\partial_t A, w')_{\Omega_c} + (\sigma \text{grad}\, \nu, w')_{\Omega_c} + < n \times H, w' >_{\Gamma_h - \Gamma_t}$$
$$+ < [n \times H]_{\Gamma_t}, w' >_{\Gamma_t} = (J, w')_{\Omega_s}, \forall\, w' \in H^1(\Omega) \tag{20}$$

Notations of $(.,.)_\Omega$ and $<.,.>_{\Gamma_h}$ are the volume and surface integrals, respectively, where the volume integral is defined in Ω and the surface integral is defined on Γ. The function space $H^1(\Omega)$ contains the test function w' and basis functions for A. At the discrete level, this function is determined by edge finite elements (FEs), which are a type of numerical discretization technique used to approximate the solution of partial differential equations. The boundary $< n \times H, w' >_{\Gamma_h - \Gamma_t}$ in (20) represents the natural BCs of (15), typically zero. From (20), by taking $w' = \text{grad}\, \nu'$ as a test function in the weak formulation (15), one gets (21).

$$(\sigma\partial_t A, grad\, \nu')_{\Omega_c} + (\sigma grad\, \nu, grad\, \nu')_{\Omega_c} + < [n \times h_i]_{\Gamma_t}, w' >_{\Gamma_t}$$
$$= < n \cdot j, \nu' >_{\Gamma_g}, \forall\, w' \in H^1(\Omega) \tag{21}$$

Where Γ_g is one of the surfaces $\Gamma_{g,i}$, which is fixed by a current or voltage as shown in Figure 2.

3.3. Coupled to voltage quantity

The voltage applied (V_i) to the inductor can be expressed as a natural global constraint via an unit source electric scalar potential $\nu_{s,i}$ associated with the applied voltage. The voltage applied to each massive inductor ($\Omega_{g,i}$) is expressed as a sum of the applied voltages between the electrodes Γ_g^+ and Γ_g^-. This results in an equation expressed as the circuit relation associated with the inductor $\Omega_{m,i}$ via the voltage V_i [4], [25]

$$\nu_i = \sum_i V_i \nu_{s,i} \tag{22}$$

By substituting (17) into (16), one gets (23).

$$\left(\frac{1}{\mu} curl\, A, curl\, w'\right)_\Omega + (\sigma\partial_t A, w')_{\Omega_c} + \sum_i V_i \ (\sigma grad\, \nu_{s,i}, w')_{\Omega_c} + < n \times H, w' >_{\Gamma_h - \Gamma_t}$$
$$+ < [n \times H]_{\Gamma_t}, w' >_{\Gamma_t} = (J, w')_{\Omega_s}, \forall\, w' \in H^1(\Omega) \tag{23}$$

3.4. Computation of Joule power losses via a post-processing

Joule losses are then computed with [21], [22]:

$$P_{loss} = \frac{1}{2}\int_\Omega \frac{J\bar{J}}{\sigma} d\Omega \tag{24}$$

where $\bar{J}$ is the conjugate of J. By using the Poynting theorem associated to the surface integration of degrees of freedom of A and ν located on the border, the volume integration can be defined as (25).

$$P_{loss} = \frac{1}{2} Re\left(\oint_{\Gamma} (n \times H) \cdot \bar{E} d\Gamma\right) = Re\left(-\frac{j\omega}{2}\oint_{\Gamma} (n \times H_s - n \times grad\ v).\bar{A} d\Gamma\right) \quad (25)$$

Where E and A are respectively the complex conjugates of electric field $\bar{E}$ and magnetic vector $\bar{A}$.

4. APPLICATION TEST

The test problem is herein a three phase SR as pointed out in Figure 3, where Figure 3(a) illustrates the representation of the air gaps between core blocks, Figure 3(b) describes the winding structure and Figure 3(c) depicts the structure of a three phase SR with the winding and magnetic circuit. The main parameters given in Table 1. The 3D model of the SR is established as in Figure 4, where a full 3D model is given in Figure 4(a). Due to the symmetric nature of the structure of the SR, in order to reduce computational time, a half cross-sectional model is considered in Figure 4(b), and imput parameters for constructing the model are pointed out in Figure 4(c).

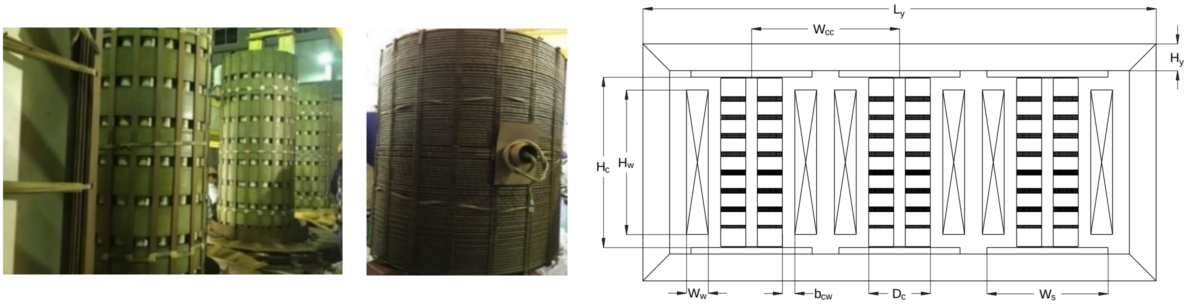

(a) (b) (c)

Figure 3. Geometry of a three phase SR (a) air gaps between core blocks, (b) winding structure, and (c) construction of a a three phase SR

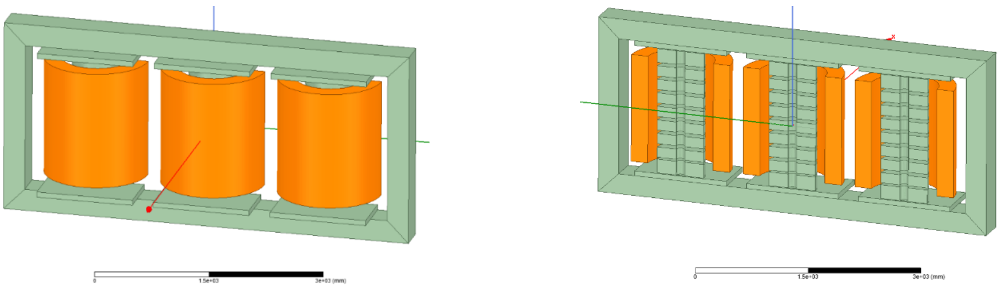

(a) (b)

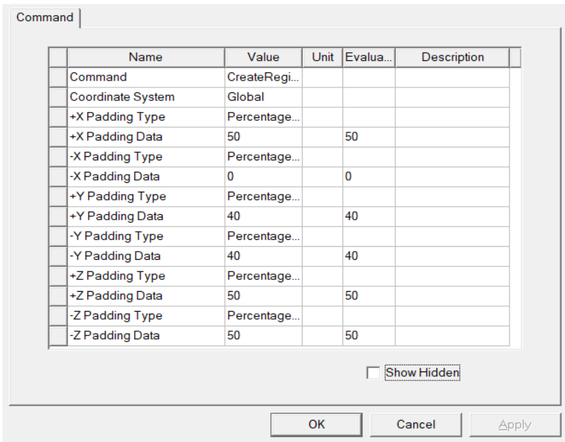

Command

Name	Value	Unit	Evalua...	Description
Command	CreateRegi...			
Coordinate System	Global			
+X Padding Type	Percentage...			
+X Padding Data	50		50	
-X Padding Type	Percentage...			
-X Padding Data	0		0	
+Y Padding Type	Percentage...			
+Y Padding Data	40		40	
-Y Padding Type	Percentage...			
-Y Padding Data	40		40	
+Z Padding Type	Percentage...			
+Z Padding Data	50		50	
-Z Padding Type	Percentage...			
-Z Padding Data	50		50	

Show Hidden

OK Cancel Apply

(c)

Figure 4. 3D-model of a three phase SR (a) 3D model of SR, (b) a half cross-sectional model, and (c) input parameters

Table 1. Parameters of the SR

Parameter	Symbol	Value	Parameter	Symbol	Value
Reactive power	Q (MVAr)	91	Deep Yoke	D_y (mm)	776
Rated current	I (A)	105	Total air gap length along the core	l_g (mm)	400
Rated voltage	U (kV)	500	Number of turns	N (vòng)	2244
Inductance	X_L (Ω)	2712	Distance between the core and windings	b_{cw} (mm)	135
Core diameter	D_c (mm)	666	Yoke width	W_w (mm)	236
Core height	H_c (mm)	1978	Winding height	H_w (mm)	1559

The distribution of phase voltage in the windings is shown in Figure 5. It shows that the effective voltage applied to windings (phase A, phase B, and phase C) is the rated phase voltage with the value of 288,675 kV, which is close to the measured result of 288,7567 kV. This means that the significant error on the voltage simulation is less than 1%.

In the same way, the phase current distribution in the winding is presented in Figure 6. The comparison of current and voltage values between the simulated and measured results is given in Table 2, with errors being lower than 1% for both cases. The magnetic flux density distribution in the magnetic circuit is presented in Figure 7. It can be shown that the value is the biggest when the current of phase B is the maximum. The magnetic flux density distribution along the line of C1-C2 (core block) is presented in Figure 8. It shows that the magnetic flux mostly focuses on the surface of the core blocks, thus the magnetic flux density near edges of the core blocks is bigger than the one inside core blocks. In order to increase the leakage flux in the vicinity of the core blocks, the reluctance of magnetic circuit and number of air gap core blocks need to increase also.

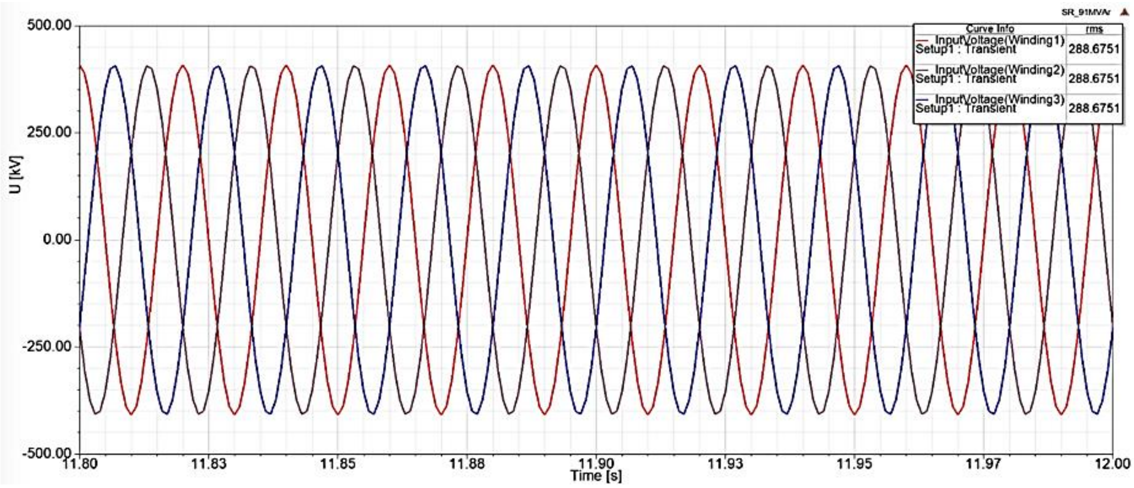

Figure 5. Voltage distribution in winding

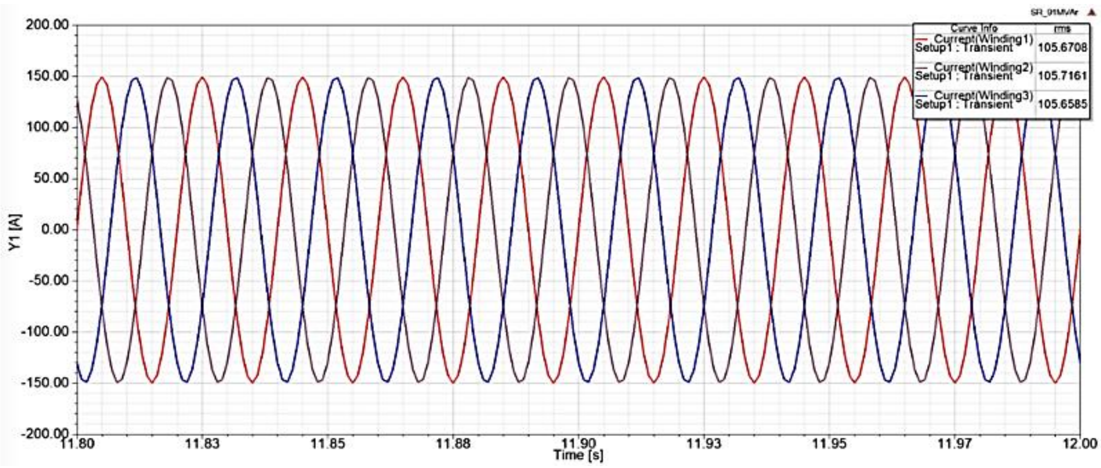

Figure 6. Current distribution in winding

Table 2. Comparison of simulated and measured voltages

Parameters	Rated values	Simulated results	Measured results	Error (%)
Current of phase A (A)	105	105.67	106.44	0.73
Current of phase B (A)	105	105.71	106.86	1.08
Current of phase C (A)	105	105.65	106.34	0.65
Voltage of phase A (V)	105	288.62	288.76	0.35
Voltage of phase B (V)	105	288.56	288.71	0.5
Voltage of phase C (V)	105	288.62	288.93	0.12

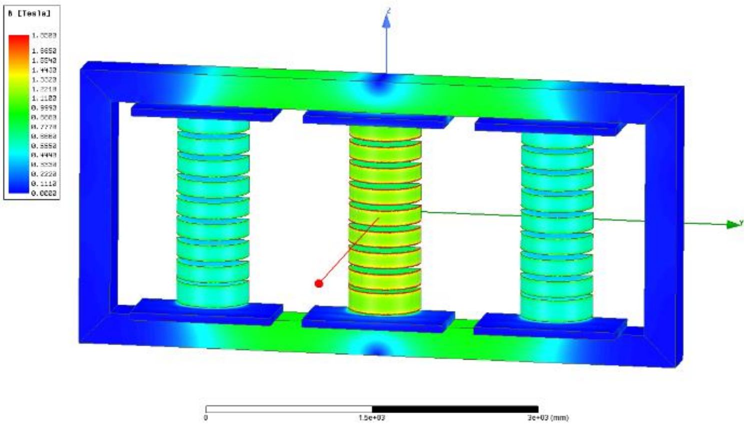

Figure 7. Distribution of magnetic flux density in the magnetic circuit

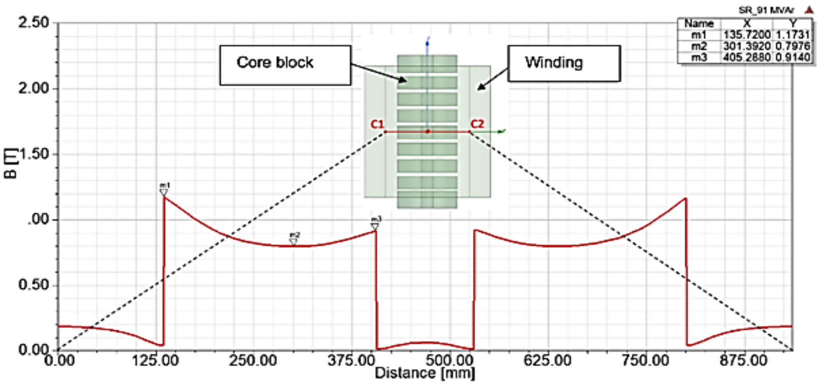

Figure 8. Distribution of magnetic flux density along the line of C1-C2 (core block)

The magnetic flux density distribution along the air gap (G1-G2) between core blocks is indicated in Figure 9. The results show that the magnetic flux density along the inner winding surface is very small and uniform due to the large number of air gaps. Its mean value is equal to 0.1797 T. The values of self and mutual inductances between phases (phase A, phase B, and phase C) are given in Table 3. The comparison of phase reactances between the rated and simulated results is given in Table 4. It can be seen that the error is lower than 1% for phase B and equal to 1% for phase A and phase C. In the same way, Table 5 shows the comparison of simulated and measured reactances for three phases. The errors on them are smaller than 2%. This is a good agreement with the developed method. In particular, it is satisfied the IEC 60076-6 of the SR. The copper and iron losses of the SR are pointed out in Figures 10 and 11, respectively. The results of iron and copper losses in the SR between the simualtion and measurement are given in Table 6. The error is lower than 4% for the iron loss and 2% for the copper loss. These errors are completely acceptable and realiable.

Table 3. The values of self and mutual inductances (H)

Inductance (H)	Phase A	Phase B	Phase C
Phase A	8.7257	-0.00565	-0.00129
Phase B	-0.00565	8.7199	-0.00566
Phase C	-0.00129	-0.00566	8.7268

Table 4. Comparison of simulated and rated reactances

Parameters	Rated value (ohm)	Simulated result (ohm)	Error (%)
Reactance (phase A)	2,712	2,739.08	1.00
Reactance (phase B)	2,712	2,735.88	0.88
Reactance (phase C)	2,712	2,739.42	1.00

Table 5. Comparison of simulated and measured reactances

Parameters	Simulated result (ohm)	Measured result (ohm)	Eror (%)
Reactance (phase A)	2,739.08	2,698.7	1.47
Reactance (phase B)	2,735.88	2,694.4	1.52
Reactance (phase C)	2,739.42	2,689.3	1.83

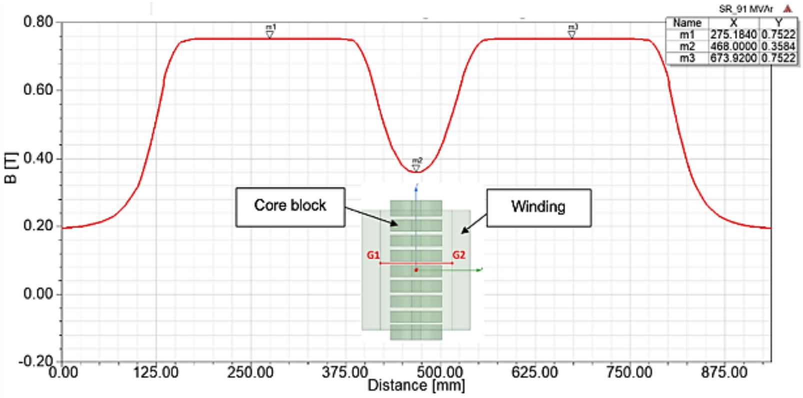

Figure 9. Magnetic flux density along the air gap (G1-G2) between core blocks

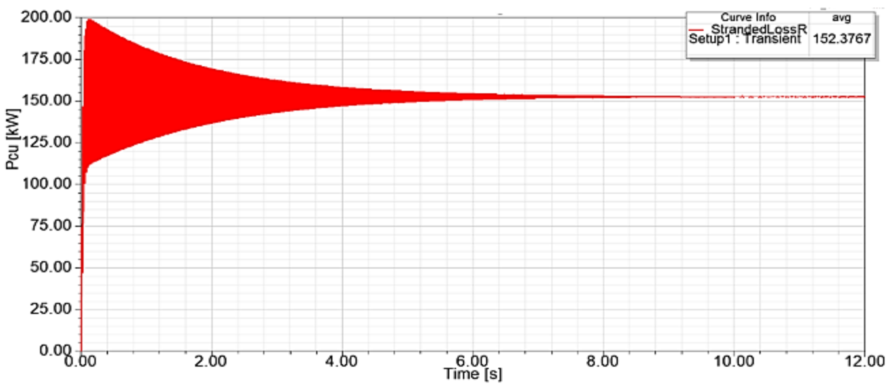

Figure 10. Copper loss in the winding of the SR

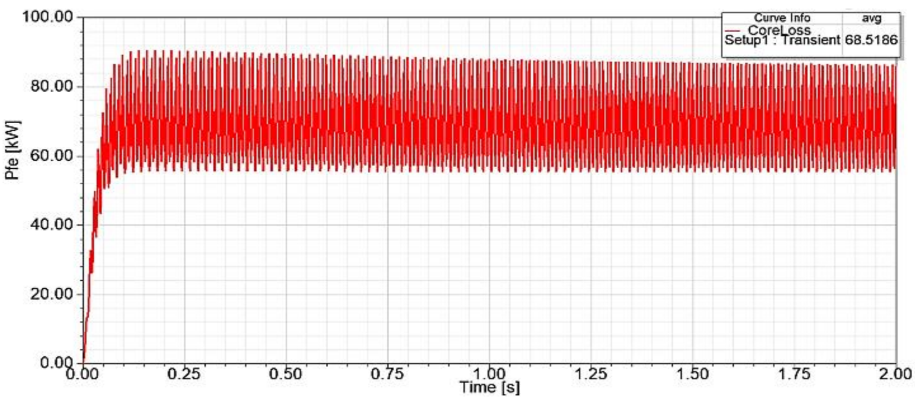

Figure 11. Iron loss in the magnetic circuit of the SR

Table 6. Comparison of simulated and measured copper and iron losses

Parameters	Simulated result (kW)	Measured result (kW)	Error (%)
Iron loss	68.519	70.817	3.24
Coppeer loss	152.377	155.321	1.90

5. CONCLUSION

In this research, the proposed SR was designed using an analytical approach to determine its main parameters. Afterward, a FEM simulation was conducted to simulate the prototype of the SR. The results of the SR obtained from the FEM were then compared to the that from the measured method to confirm their accuracy. The obtained results have also suggested that the analytical approach and FEM simulation are accurate methods for calculating various parameters of the SR. These parameters include voltage, current, inductance, reactance, copper loss, and iron loss. Additionally, these methods can also evaluate material costs, losses and other critical parameters. Moreover, the use of FEM simulation allows for a faster design and computing process and to optimize the prototypes needed to achieve the expected results. This approach can potentially save time and cost in the design and manufacturing of shunt reactors.

REFERENCES

[1] T. P. Minh *et al.*, "Finite Element Modeling of Shunt Reactors Used in High Voltage Power Systems," *Engineering, Technology & Applied Science Research*, vol. 11, no. 4, pp. 7411–7416, Aug. 2021, doi: 10.48084/etasr.4271.

[2] H. B. Duc, T. P. Minh, T. P. Anh, and V. D. Quoc, "A Novel Approach for the Modeling of Electromagnetic Forces in Air-Gap Shunt Reactors," *Engineering, Technology & Applied Science Research*, vol. 12, no. 1, pp. 8223–8227, Feb. 2022, doi: 10.48084/etasr.4692.

[3] T. P. Minh, H. B. Duc, and V. D. Quoc, "Analysis of Leakage Inductances in Shunt Reactors: Application to High Voltage Transmission Lines," *Engineering, Technology & Applied Science Research*, vol. 12, no. 3, pp. 8488–8491, Jun. 2022, doi: 10.48084/etasr.4826.

[4] Z. Wei-jie, Z. Xiao-xin, L. Ya-lou, Z. Xing, and X. De-chao, "Inverse-Hyperbolic Dynamic Model for Extra and Ultra Voltage Magnetically Controlled Shunt Reactor," in *2010 International Conference on Electrical and Control Engineering*, Jun. 2010, pp. 2820–2823, doi: 10.1109/iCECE.2010.689.

[5] Y. Hao, X. Yonghai, L. Yingying, Z. Yongqiang, and X. Xiangning, "Study of Nonlinear Model of Shunt Reactor in 1000kV AC Transmission System," in *2009 International Conference on Energy and Environment Technology*, 2009, pp. 305–308, doi: 10.1109/ICEET.2009.312.

[6] P. Mestas, M. C. Tavares, and A. M. Gole, "Implementation and Performance Evaluation of a Reclosing Method for Shunt Reactor-Compensated Transmission Lines," *IEEE Transactions on Power Delivery*, vol. 26, no. 2, pp. 954–962, Apr. 2011, doi: 10.1109/TPWRD.2010.2084111.

[7] G. W. Chang, H. M. Huang, and J.-H. Lai, "Modeling SF6 Circuit Breaker for Characterizing Shunt Reactor Switching Transients," *IEEE Transactions on Power Delivery*, vol. 22, no. 3, pp. 1533–1540, Jul. 2007, doi: 10.1109/TPWRD.2007.899799.

[8] A. Lotfi and E. Rahimpour, "Optimum design of core blocks and analyzing the fringing effect in shunt reactors with distributed gapped-core," *Electric Power Systems Research*, vol. 101, pp. 63–70, Aug. 2013, doi: 10.1016/j.epsr.2013.03.006.

[9] K. Dawood, G. Komurgoz, and F. Isik, "Modelling of the Shunt Reactor by using Finite Element Analysis," in *2020 XI International Conference on Electrical Power Drive Systems (ICEPDS)*, Oct. 2020, pp. 1–5, doi: 10.1109/ICEPDS47235.2020.9249363.

[10] D. Q. Vuong and N. D. Quang, "Coupling of Local and Global Quantities by A Subproblem Finite Element Method – Application to Thin Region Models," *Advances in Science, Technology and Engineering Systems Journal (ASTESJ)*, vol. 4, no. 2, pp. 40–44, 2019.

[11] S. Pokharel and A. Dimitrovski, "Analytical Modeling of A Ferromagnetic Core Reactor," in *2019 North American Power Symposium (NAPS)*, Oct. 2019, pp. 1–6, doi: 10.1109/NAPS46351.2019.9000352.

[12] R. Jez, "Influence of the Distributed Air Gap on the Parameters of an Industrial Inductor," *IEEE Transactions on Magnetics*, vol. 53, no. 11, pp. 1–5, Nov. 2017, doi: 10.1109/TMAG.2017.2699120.

[13] Y. G. Zhang, K. X. Chang, and Y. C. Su, "Shunt Reactors Compensation Research of UHV Accessed to Jiangxi Power Grid," *Advanced Materials Research*, vol. 1070–1072, pp. 1029–1034, Dec. 2014, doi: 10.4028/www.scientific.net/AMR.1070-1072.1029.

[14] A. Y. Arabul, E. Kurt, I. Senol, and F. K. Arabul, "An ınvestigation on flux density of three phase distributed Air-Gap 3-5 legged shunt reactor," *IRES-27th ICIET*, 2015.

[15] J. Ning, H. Baoxing, Z. Ruoyu, M. Hongzhong, X. Lei, and L. Li, "Application of Empirical Wavelet Transform in Vibration Signal Analysis of UHV Shunt Reactor," in *2019 IEEE Milan PowerTech*, Jun. 2019, pp. 1–5, doi: 10.1109/PTC.2019.8810623.

[16] K. Dawood, G. Komurgoz, and F. Isik, "Modeling of Distribution Transformer for Analysis of Core Losses of Different Core Materials Using FEM," in *2019 8th International Conference on Modeling Simulation and Applied Optimization (ICMSAO)*, Apr. 2019, pp. 1–5, doi: 10.1109/ICMSAO.2019.8880392.

[17] M. Mu, F. Zheng, Q. Li, and F. C. Lee, "Finite Element Analysis of Inductor Core Loss Under DC Bias Conditions," *IEEE Transactions on Power Electronics*, vol. 28, no. 9, pp. 4414–4421, Sep. 2013, doi: 10.1109/TPEL.2012.2235465.

[18] F. Zhang, S. Ji, Y. Shi, and L. Zhu, "Investigation on the Action of Eddy Current on Tank Vibration Characteristics in Dry-Type Transformer," *IEEE Transactions on Magnetics*, vol. 55, no. 2, pp. 1–8, Feb. 2019, doi: 10.1109/TMAG.2018.2883854.

[19] R. Yan *et al.*, "Research on Three-Dimensional Stress Distribution of Reactor Core," *IEEE Transactions on Applied Superconductivity*, vol. 26, no. 4, pp. 1–4, Jun. 2016, doi: 10.1109/TASC.2016.2527048.

[20] B. Tong, Y. Qingxin, Y. Rongge, Z. Lihua, and C. Junjie, "Stress Analysis of Inverter-Fed Induction Motor Considering Anisotropic Magnetization and Magnetostrictive Properties," *IEEE Transactions on Applied Superconductivity*, vol. 28, no. 3, pp. 1–4, Apr. 2018, doi: 10.1109/TASC.2017.2786242.

[21] G. Zhang, J. Wu, and L. Hao, "Fast Calculation Model and Theoretical Analysis of Rotor Unbalanced Magnetic Pull for Inter-Turn Short Circuit of Field Windings of Non-Salient Pole Generators," *Energies*, vol. 10, no. 5, p. 732, May 2017, doi: 10.3390/en10050732.

[22] X. Xu, Q. Han, and F. Chu, "Review of Electromagnetic Vibration in Electrical Machines," *Energies*, vol. 11, no. 7, p. 1779, Jul. 2018, doi: 10.3390/en11071779.

[23] A. Deihimi, "Improved model of saturated regions in Magnetic Equivalent Circuits of highly saturated electromagnetic devices," in *2008 11th International Conference on Optimization of Electrical and Electronic Equipment*, May 2008, pp. 45–50, doi: 10.1109/OPTIM.2008.4602385.

[24] M. Amrhein and P. T. Krein, "3-D Magnetic Equivalent Circuit Framework for Modeling Electromechanical Devices," *IEEE Transactions on Energy Conversion*, vol. 24, no. 2, pp. 397–405, Jun. 2009, doi: 10.1109/TEC.2009.2016134.

[25] B. Tong, Y. Qingxin, Y. Rongge, and Z. Lihua, "Magnetically Controlled Saturable Reactor Core Vibration Under Practical Working Conditions," *IEEE Transactions on Magnetics*, vol. 53, no. 6, pp. 1–4, Jun. 2017, doi: 10.1109/TMAG.2017.2664104.

BIOGRAPHIES OF AUTHORS

Hung Bui Duc received his engineer degree in Electrical engineering from Hanoi University of Science and Technology, Viet Nam, in 1989, and his doctor degree in Electrical engineering from Hanoi University of Science and Technology, Viet Nam in 1999. He is currently working as a team leader of electrical machines's group, and also a lecturer of Department of Electrical Engineering, School of Electrical Engineering, Hanoi University of Science and Technology. His research domain encompasses electrical machines (transformers, motors and shunt reactors) and numerical methods. He can be contacted at email: hung.buiduc@hust.edu.vn.

Tu Pham Minh received his engineer degree in Electrical engineering from Hanoi University of Science and Technology, Viet Nam, in 2009, his master degree in Electrical engineering from Hanoi University of Science and Technology, Viet Nam in 2011, and his Ph.D. degree in Electrical engineering from Hanoi University of Science and Technology, Viet Nam in 2022. He is currently working as a lecturer at the Department of Electrical Engineering, School of Electrical Engineering, Hanoi University of Science and Technology. His research domain encompasses electrical machines electrical machines (transformers, motors and shunt reactors) and numerical methods. He can be contacted at email: tu.phamminh@hust.edu.vn.

Bao Doan Thanh received the B.S. degree in Electrical engineering from Hanoi University of Science and Technology, Viet Nam, in 2006, the M.S. degree from Hanoi University of Science and Technology, Viet Nam, in 2010 and the Ph.D. degree from Hanoi University of Science and Technology, in 2016. He is currently working as a lecturer at Faculty of Engineering and Technology, Quy Nhon University, Viet Nam. His research interests include electrical power system, switching devices, electrical machines and transformers; calculation of magnetic fields an electromagnetic. He can be contacted at email: doanthanhbao@qnu.edu.vn.

Duc-Quang Nguyen received his Ph.D. degree in 2013 from the Ecole Nationale Superieure d'Arts et Metiers Paristech, France. He is currently working as a lecturer at the Faculty of Electrical Engineering, Electric Power University. His research domain encompasses modeling of electromagnetic systems and electrical machines. He can be contacted at email: quangndhtd@epu.edu.vn.

Vuong Dang Quoc received his Ph.D. degree in 2013 from the Faculty of Applied Sciences at the University of Liège in Belgium, and his associate professor at the state council for professor, Viet Nam, in 2020. He is currently working as a deputy director of Training Center of Electrical and Electronic Engineering, School of Electrical and Electronic Engineering, Hanoi, University of Science and Technology. His research domain encompasses modeling of electromagnetic systems and electrical machines, thin shells, and numerical methods. He can be contacted at email: vuong.dangquoc@hust.edu.vn.